Turbulent Coherent Structures under Breaking Water Waves

Rozita Jalali Farahani
Civil Engineering Department
Johns Hopkins University
Baltimore, USA
rozita@jhu.edu

Robert A. Dalrymple
Civil Engineering Department
Johns Hopkins University
Baltimore, USA
rad@jhu.edu

Alexis Hérault
Conservatoire National des Arts et Métier
Paris, France
alexis.herault@cnam.fr

Giuseppe Bilotta
Università degli studi di Catania
Catania, Italy
bilotta@dmi.unict.it

Abstract—**The nature of wave breaking at beaches and the subsequent three-dimensional turbulence under the waves are of great interest in coastal engineering. The breaking waves were modelled on a slope using the 3-D open-source GPUSPH code of Hérault, Bilotta and Dalrymple (2010). Then, different coherent structure detection methods were employed, including vorticity, Q criterion, and λ_2 criterion. These last two criteria are based on the velocity gradient tensor and its symmetric and anti-symmetric components. The evolution of the turbulence under a plunging wave is discussed. For plunging waves, the plunger touch-down, the jet penetration, and subsequent splash-up are all sources of vorticity.**

I. INTRODUTION

The characteristics of wave breaking in the surf zone has been of great interest for coastal engineers and fluid dynamicists. As ocean waves propagate towards shore they undergo shoaling, shortening in length and increasing in height. As the waves enter the diminishing water depths close to the beach, waves break, leading to splash-up, and white water fronts or spray depending on the nature of the waves. There are four different generic breaker types: spilling, plunging, collapsing and surging waves, depending on the initial steepness of the waves and the steepness of the beach slope [1].

- In spilling waves, when the wave crest becomes unstable, it spills forward and creates white water in front of the wave and the wave energy is dissipated in this turbulent white water. Spilling waves usually occur on gradual beach slopes.
- In plunging waves, the crest of the wave becomes very steep--almost vertical, then it overturns as a jet and falls into the water in front of the wave, followed by a splash-up, which is sometimes higher than the original wave. Depending on the position of the first plunging point, a sequence of plunging and overturning jets appear in front of the initial wave. This splash-up cycle produces vortex structures propagating towards the shore.
- In collapsing waves, the lower part of the wave gets steeper and curls over, following by bubbles and foam.
- For surging waves, which appear on very steep beaches, the lower part of the wave moves rapidly forward and the wave crest does not curl over. There is no turbulent breaking process.

Several laboratory and numerical studies demonstrated that the turbulent flow under the breaking wave could be characterized by large-scale flow structures, which are called coherent structures. Nadaoka, Hino and Koyano [2] performed a set of laboratory experiments to examine the breaking wave dynamics and the generated turbulence structure. They studied the three-dimensional eddies found under and behind the wave crest, called obliquely descending eddies. Ting [3] studied a solitary wave experimentally and captured coherent structures under the breaking wave, which were the sources of turbulent energy. Watanabe, Saeki and Hosking [4] modelled the large-scale vortex structures under spilling and plunging waves using large eddy simulation (LES) method. Three dimensional vortex structures were captured in both plunging and spilling waves. They studied the obliquely descending eddies, which have an important role in sediment transportation and beach erosion.

In this study, generation and evolution of Lagrangian three-dimensional coherent structures under the plunging water waves are numerically modelled using SPH (Monaghan, 1994), specifically the GPUSPH model developed by Hérault, Bilotta and Dalrymple (2010) [5], [6]. The Navier-Stokes equations are numerically solved using a turbulence closure model to consider small-scale eddies as well.

II. COHERENT STRUCTURES

In this section, we briefly outline some definitions related to the vortex and coherent structures in fluid mechanics. Study of spatially coherent, time-depending vortex structures has an important role on the understanding of turbulent flow physics. Several researchers have

proposed different definitions of "vortex". Brachet, Meneguzzi, Politano and Sulem (1988) defined a vortex as a region of negative velocity gradient determinant [7]. Babiano, Basdevant, Legras and Sadourny (1987) defined a vortex any region of a fluid with vorticity magnitude greater than a specific threshold [8]. McWilliams (1990) proposed a quantitative definition and recognized a vortex as a fluid region that is bounded by vorticity magnitude equal to 20% of the local extremum of vorticity magnitude [9]. Green [10] defined a fluid vortex as any region of concentrated vorticity. Although this definition has some ambiguities, it has been used in a wide variety of studies.

A vortex line is a line that is everywhere tangent to the local vorticity vector. This definition is analogous to the streamline, which is a line that is tangent to the local velocity vector. A vortex tube is the set of all vortex lines passing through a specific closed surface. Coherent structures are vortex structures that separate the fluid field to distinct regions, which are rotating relative to each other and can be of any shape. Robinson (1991) defined vortical structures as regions of flow with low pressure. In a rotating motion, pressure tends to have a local minimum on the axis of rotation since the centrifugal force needs to be balanced by pressure. This definition may not capture all vortical regions of the flow since a single pressure threshold can not reveal all spanwise and streamwise vortical structures. The vorticity magnitude can be used to detect vortex cores but it has been proved to misdetect vortical structures in some fluid flows. For instant, in some wall-bounded flows, the maximum of vorticity magnitude occurs at the wall, although there is no rotating motion close to the wall [11].

Hunt, Wray and Moin (1988) [12] proposed a vortex criteria using velocity gradient decomposition to symmetric and antisymmetric components as in equation (1).

$$\nabla\vec{v} = S + \Omega \tag{1}$$

where S is rate of strain tensor and Ω is the rotation tensor.

These two tensors are calculated as:

$$S = \frac{1}{2}[\nabla\vec{v} + (\nabla\vec{v})^T] \tag{2}$$

$$\Omega = \frac{1}{2}[\nabla\vec{v} - (\nabla\vec{v})^T] \tag{3}$$

According to their definition, a vortex structure is a spatial region where the following criteria, which is called Q criteria, is satisfied:

$$Q = \frac{1}{2}[|\Omega|^2 - |S|^2] > 0 \tag{4}$$

Jeong and Hussain (1995) [11] defined a vortex core as a flow region with following two conditions:

(1) A vortex core must have a net circulation and vorticity.

(2) A vortex core should have a Galilean invariant geometry.

In order to meet the previous conditions, they proposed a new definition based on the eigenvalues of $S^2 + \Omega^2$. The main concept came from the fact that minimum of pressure occurs on the axis of rotation but this definition is not sufficient as a detection criterion. For instance unsteady irrotational straining creates a pressure minimum although no vortex exist. Therefore they removed the unsteady effects and proposed that vortex structures are connected regions where the median eigenvalue of $S^2 + \Omega^2$ is negative:

$$\lambda_1 \geq \lambda_2 \geq \lambda_3 \tag{5}$$

$$\lambda_2 < 0 \tag{6}$$

$S^2 + \Omega^2$ is a real symmetric tensor so it has only real eigenvalues. By definition the negative median eigenvalue of this tensor demonstrates the vortex structures.

III. NUMERICAL MODELING OF PLUNGING WATER WAVE

A. Numerical model

Modeling breaking water waves with SPH was begun by Monaghan [5] in 1994. Dalrymple and Rogers [14] examined 3D breaking waves in the surf zone, showing that the breaking wave is the source of considerable vorticity.

Here a plunging water wave was numerically modelled using GPUSPH [6] model, which is an open-source SPH code available from www.ce.jhu/dalrymple/GPUSPH. In this code, the CUDA programming language is used to implement SPH calculations on the Graphic Processing Units (GPUs) of computers instead of Central Processing Units (CPUs). SPH has a data parallel nature and it performs very well on GPUs, which have a parallel architecture.

The governing equations are the Navier-Stokes equation that is written as follows:

$$\frac{1}{\rho}\frac{D\rho}{Dt} + \nabla.\vec{u} = 0 \tag{7}$$

$$\frac{D\vec{u}}{Dt} = \frac{1}{\rho}\nabla P + \frac{1}{\rho}\nabla.\vec{T} + \vec{g} \tag{8}$$

where ρ = fluid particle density; $\vec{u}$ = particle density; P = fluid particle pressure; $\vec{T}$ = viscous stress tensor and $\vec{g}$ = gravity vector.

A weakly compressible SPH formulation is rendered in particle form for use in GPUSPH and particle pressure is calculated from the equation of state [5], [6]. Different boundary conditions are applied in this model: (1) Lennard-Jones forces between boundary particles and fluid particles, which prevent the fluid particles from penetrating into boundary particles and (2) Monaghan and Kajtar (2009) boundary condition where a new form of radial boundary forces are introduced [13].

In order to capture eddies and vortex structure under the plunging wave, a combination of SPH method and Large

Eddy Simulation (LES) called sub-particle scale (SPS) is used [14]. A LES filtering is applied to Navier-Stokes equations to calculate large-scale eddies. Small-scale eddies are modelled using a Sub-Grid-Scale (SGS) turbulence model. The standard Smagorinsky model (1963) is used to model the small-scale eddies and the Smagorinsky coefficient is assumed to be constant over time and over space [14].

B. *Plunging wave characteristics*

A plunging wave is generated with a flap wave maker and propagates towards a beach with a slope of 1 to 5.6 (vertical to horizontal). The wave simulation is performed in a wave tank of 5.5m long, 2m wide and 3m high. The bottom of the tank has a 1m horizontal section and a 4.5m slope length. The water height in the horizontal part of the tank is equal to 0.65m. The plunging wave has a wave height of 0.45m and a wave period of 1s. Particle spacing in SPH simulation is set to be equal to 0.01m and about 4.5 million particles are used. Our numerical model simulated a five wave sequence, starting from still water in the tank. A schematic sketch of the wave tank used in the numerical model is given in figure (1). In order to apply boundary conditions, Lennard-Jones forces are used for boundary particles and a Shepard filtering is applied every 20 time steps in order to smooth the particles' density. A floating ball is situated near the wavemaker at the middle of the tank in y direction in order to illustrate the interaction between a plunging breaking wave and a floating body and its effect on the coherent structures under the breaking wave.

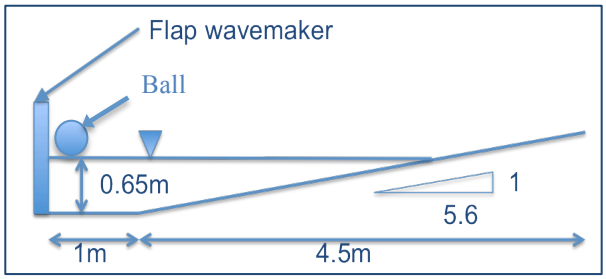

Figure 1. Schematic side view of the wave tank, showing the wavemaker and the floating ball at the water surface.

C. *Post-processing calculations*

The plunging wave is modelled by GPUSPH code [6] and velocity, vorticity and other physical parameters are calculated for moving particles in each time step using Navier-Stokes equations. In order to study the coherent turbulent structures under the breaking wave, the physical parameters of moving particles need to be mapped on fixed spatial nodes. To achieve this goal, fluid velocity on the nodes are calculated using original SPH integration formula, which is applied over the fluid parameters of nodes' neighbouring moving particles:

$$A_p = \sum_p m_p \frac{A_p}{\rho_p} W(|r_n - r_p|, h) \qquad (9)$$

where notation "n" corresponds to the fixed nodes, notation "p" corresponds to the moving particle and "A" can be any fluid parameter such as velocity, pressure or density. The fixed nodes do not contribute in the process of force calculation and they are using the existing neighbour list of particles. Therefore they do not have a significant impact on the computational expenses. Figure (2) presents a schematic of computational domain and the relation between moving particles and fixed nodes.

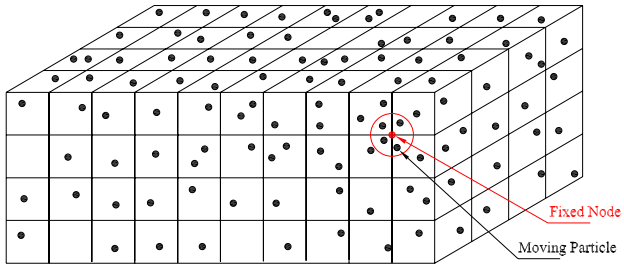

Figure 2. Schematic computational domain and the position of fixed nodes and moving particles

When velocity on each fixed node is calculated, velocity gradient tensor and its symmetric and antisymmetric components are computed. Then $\boldsymbol{Q}$ and $\boldsymbol{\lambda_2}$ values are found according to the equations mentioned in the previous section. In order to find the coherent structures, we looked at isosurfaces of positive $\boldsymbol{Q}$ and negative $\boldsymbol{\lambda_2}$

IV. NUMERICAL RESULTS OF COHERENT VORTEX FORMATION

In this section, the formation of the three-dimensional large-scale coherent structures under a plunging wave is investigated. The water wave motion is two-dimensional at the time of generation as the paddle is two-dimensional, but at breaking, when an overturning jet meets the water surface at the toe of the wave, the fluid motion becomes three-dimensional and involves various rotations along different axes. When the plunging wave curls over and hits the water, splash-up happens, which leads to another jet that jumps forward and creates another splash-up and this sequence continues with gradually decreasing scale. Formation of plunging jets and splash-ups one after another is called splash-up cycle and its length depends on the position of the first jet on the beach. Creation of coherent structures depends on the mode of the splash-up.

As the wave breaks, the plunging jet penetrates into the water surface as vertical counter-rotating eddies and the tip of the jet shapes a finger-shape surface shape. Then a horizontal roller as a spanwise rotational vortex structure is created, which moves along the wave direction. In order to capture the coherent structures related to a plunging wave, we considered a cubic window that covers the plunging wave flow and this window moves with the wave speed. Coherent structures are computed in this window. Figure

(3) shows the surface deformation for the first breaking event where the first jet is meeting the front water and the surf zone is still undisturbed. t_p is referred to the time when the first plunging wave meets the water surface ahead. Isosurfaces of negative λ_2 corresponding to the coherent structures exactly under the broken wave are illustrated in this picture. The coherent structure that covers the overturning jet has an irregular spanwise tube shape with several vertical finger-shape parts at the tow of the jet. This horizontal roller, which is rotating along the wave direction, will be developed to a regular tube when it reaches the surf zone. Figure (4) presents the vorticity magnitude and vorticity vectors on SPH particles. The vorticity vectors are mostly dominated at the point where the jet tip meets the water surface and illustrate a rotation along y direction. Some vorticity vectors are captured around the floating ball, which is being carried along the wave crest. The sequence of plunging jets and splash-ups is presented in figure (5). When the first jet curls over and falls into the water, then the downward high momentum caused by the jet push the water region in front of it forward and forms a splash-up which flows ahead as a secondary jet. The secondary jet, which is smaller in scale in comparison to the primary jet, also curls over and penetrates into the water and is followed by a splash-up. Both first and second jets cause vertical structures under their toe. Figure (6) presents an x-view of coherent structures under overturning jets.

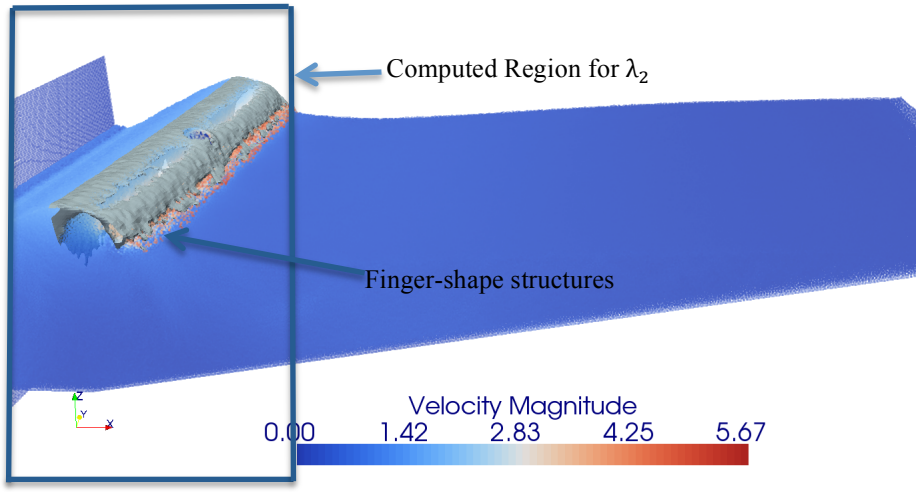

Figure 3. Wave shape and isosurfaces of $\boldsymbol{\lambda_2 = -0.2}$ at $\boldsymbol{t = t_p}$. Note: Ball is overtopped by wave at the center of the wave crest.

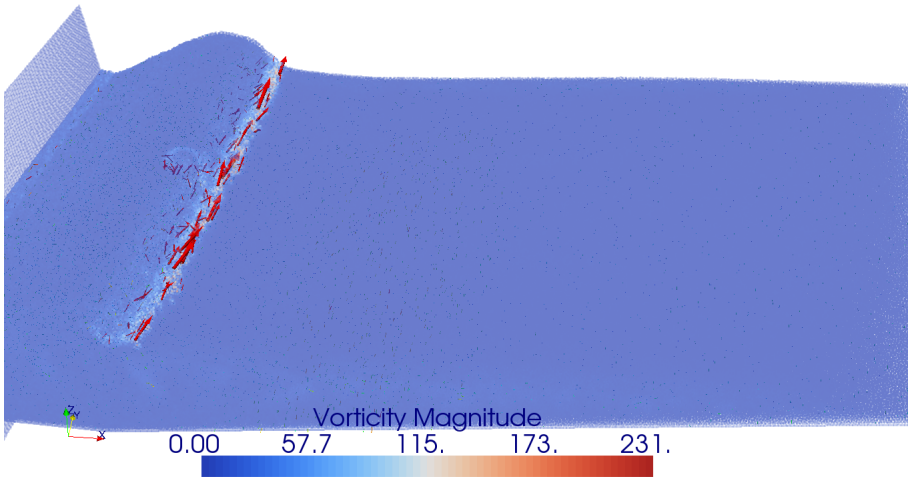

Figure 4. Particle vorticity magnitude and vorticity vectors in red at $\boldsymbol{t = t_p}$ Note: Ball is overtopped by wave at the center of the wave crest.

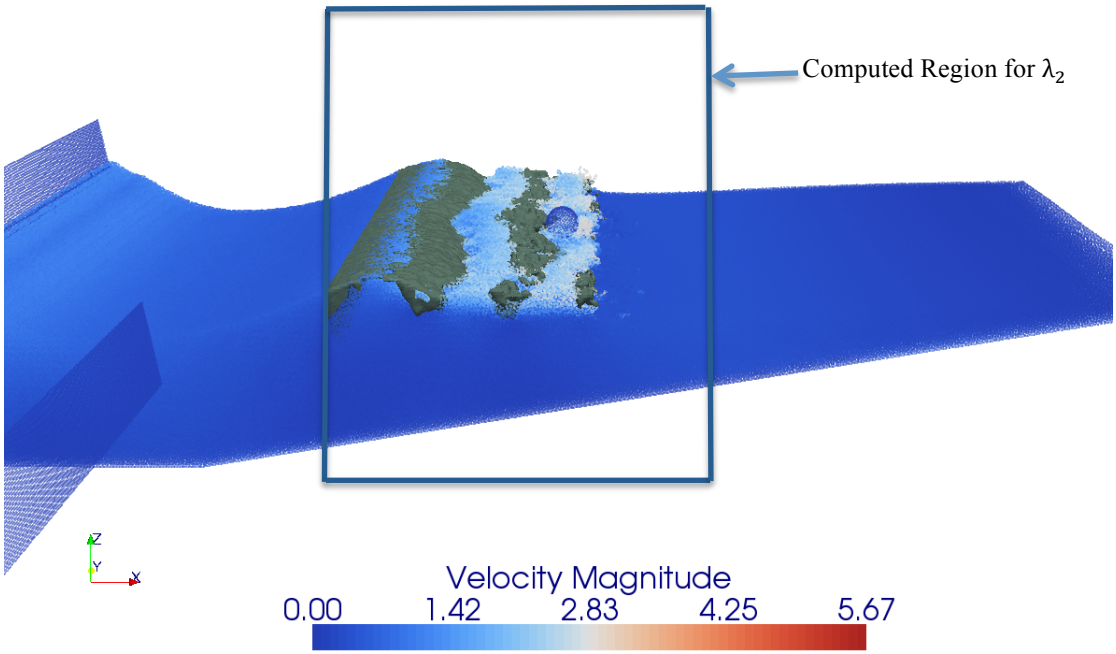

Figure 5. Side view of sequence of plunging jets and splash-up and isosurfaces of $\boldsymbol{\lambda_2 = -0.2}$ at $\boldsymbol{t = t_p + \frac{4}{10}T}$. Note the floating ball located outside of the vortex structure.

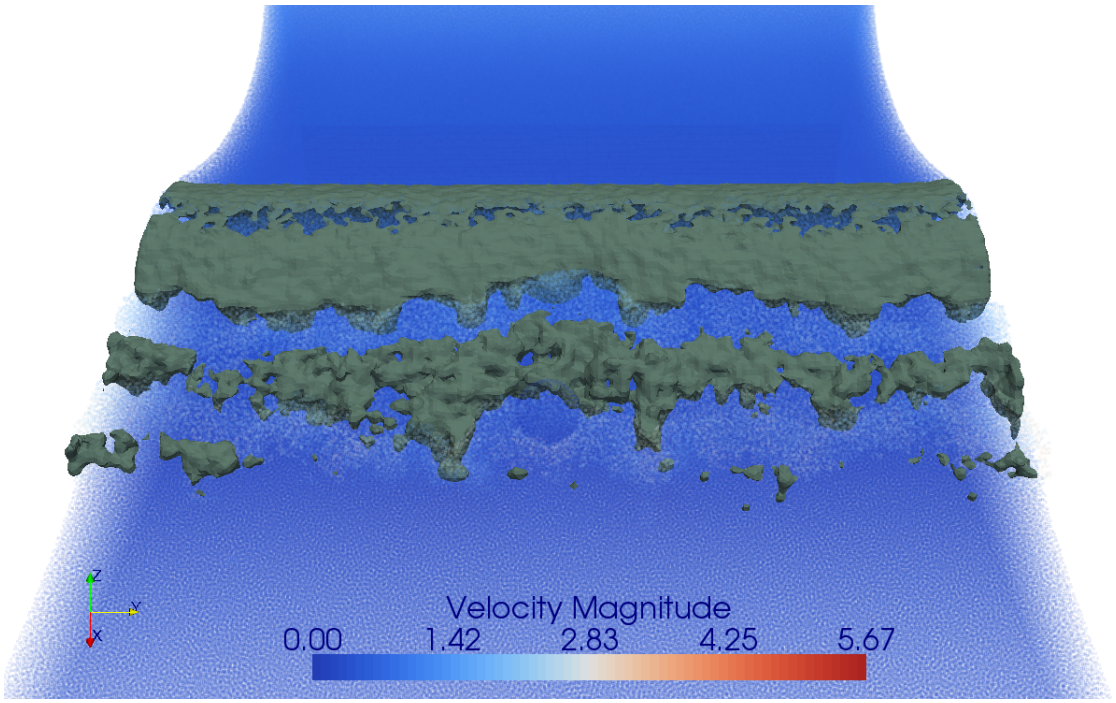

Figure 6 . x-normal view of vertical and spanwise coherent structures with isosurfaces of of $\boldsymbol{\lambda_2 = -0.2}$ at $\boldsymbol{t = t_p + \frac{4}{10}T}$

For the first jet, the vertical structures are connected to a spanwise roller, which is spread all over the width of the tank. This roller travels with the speed of the wave and in its direction. It has an irregular shape at the time of generation but after a while it develops to be a cylindrical tube.

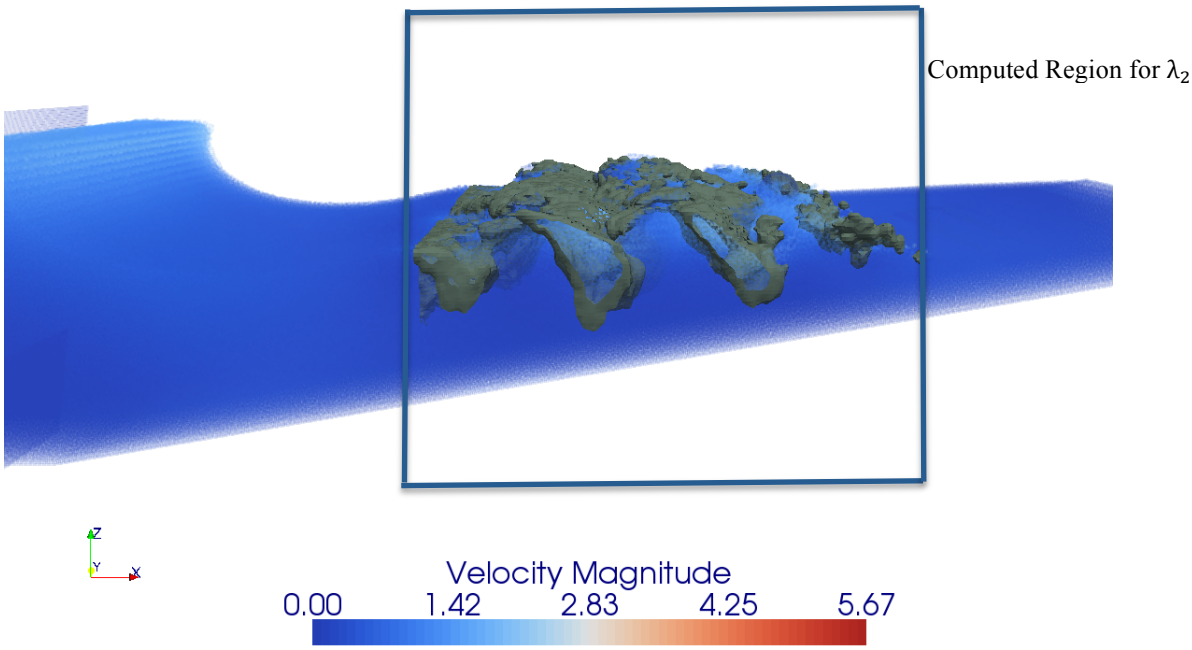

Figure 7. Side view of sequence of plunging jets and splash-up and isosurfaces of $\boldsymbol{\lambda_2 = -0.2}$ at $\boldsymbol{t = t_p + \frac{8}{10}T}$

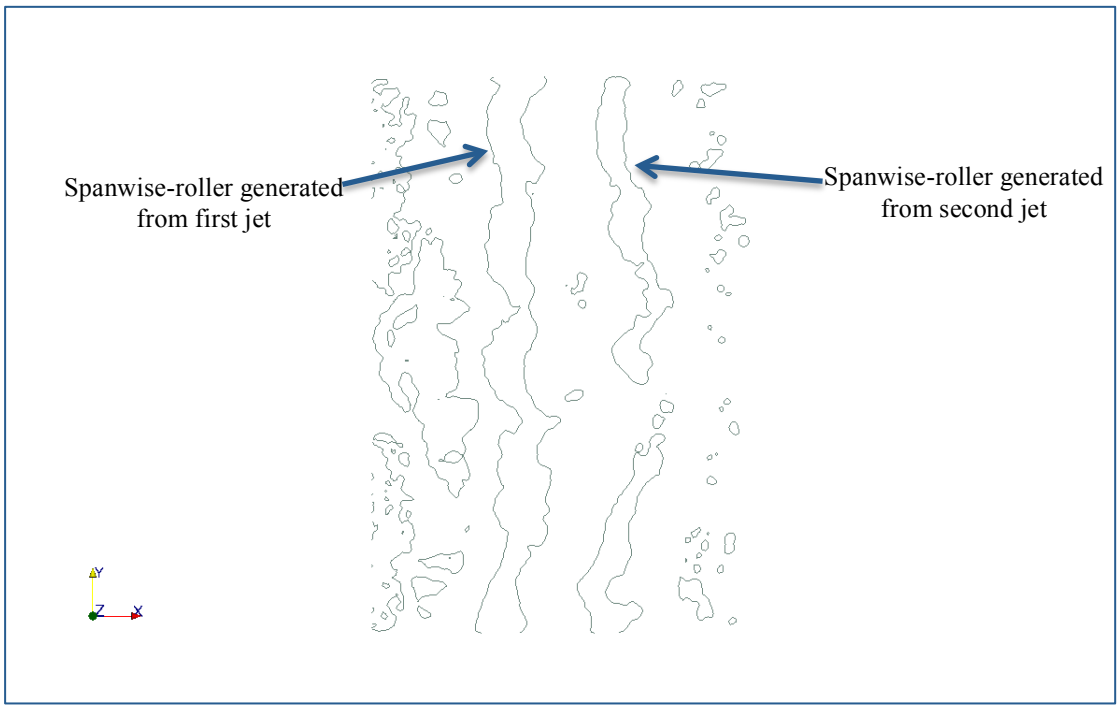

Figure 8. z-normal slide view of coherent structures with isosurfaces of $\boldsymbol{\lambda_2 = -0.2}$ at $\boldsymbol{t = t_p + \frac{8}{10}T}$, showing the irregular nature of the coherent structures.

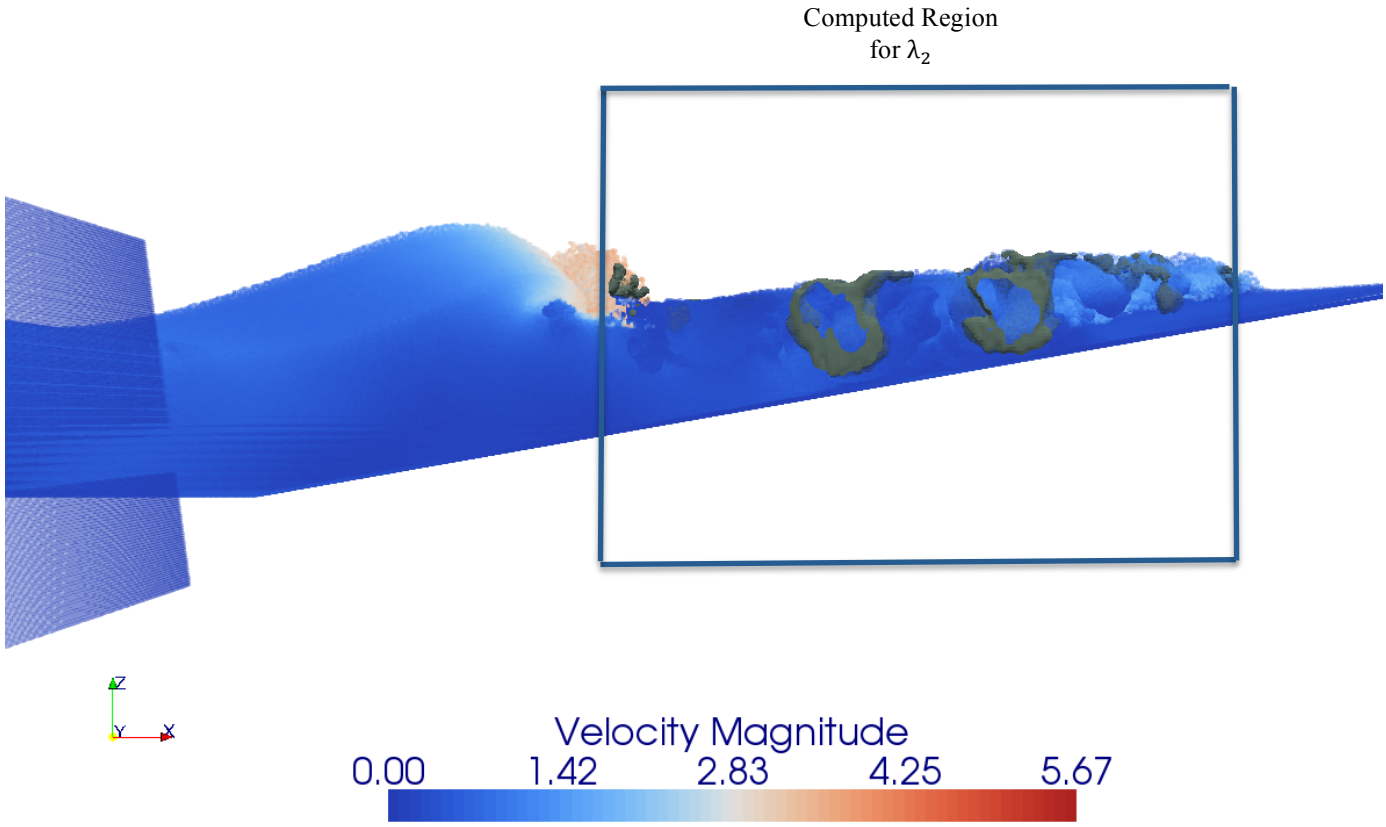

Figure 9 . Side view of sequence of plunging jets and splash-up and isosurfaces of $\boldsymbol{\lambda_2 = -0.1}$ at $\boldsymbol{t = t_p + \frac{12}{10}T}$

The second jet penetrates into the water and causes vertical vortex structures. The vertical structures generated from the second jet are also connected to each other in spanwise direction but instead of one unique horizontal structure along the width of the tank, several rollers appear at the secondary jet tow and after a while they connect to each other and create two distinct rollers. The vertical vortex structures seem to penetrate deeper around the floating body. Figure (7) shows the primary jet and secondary jet of first breaking event at time equal to $t_p + \frac{8}{10}T$. Two distinct spanwise rollers can be captured. In order to study the coherent structures more accurately, a slide has been made at the half of the water depth (z-normal), which is presented in figure (8). The horizontal roller caused by the first jet is connected along the spanwise direction. The second jet causes another horizontal roller, which is disconnected at the half of the tank in spanwise direction. This disconnection may be related to the existence of the floating body in that position. The second jet also splash up and make another jet. The third jet penetrates into the water (figure (9)). This jet has a much smaller scale in comparison to the first jet and it makes some distinct vertical vortices.

I. Conclusion

The formation of three-dimensional coherent structures under a plunging wave has been investigated by the use of GPUSPH model (Hérault, Bilotta and Dalrymple, 2010). Study of coherent structures under breaking waves can reveal the mixing and sediment transport in a beach.

To detect coherent structures, we applied λ_2 and Q criteria, which are based on strain-rate and rotation components of velocity gradient tensor. To calculate these criteria, fluid parameters of moving particles are mapped onto fixed Eulerian nodes using SPH interpolation. Then velocity gradient tensor and corresponding λ_2 and Q criteria are computed for each Eulerian node. Both λ_2 and Q criteria detect relatively similar structures but λ_2 criterion shows more clear patterns. When a plunging wave breaks, an overturning jet projects from the breaking wave crest and falls into the water surface ahead. When the jet enters the water, vertical counter-rotating vortices are

generated and these finger-shape structures are connected to a horizontal spanwise roller, which is rolling in the wave direction. The turbulence is generated and intensifies between the primary jet and the secondary jet and transferred by the horizontal roller. The second jet also causes another spanwise roller. The third jet has a significantly less power from the previous jets and it causes some distinct structures. The cycle of plunging jets and splash-up gradually diminishes in scale as it approaches the beach.

REFERENCES

[1] D. H. Peregrine, "Breaking waves on beaches", Annual Review of Fluid Mechanics, 1983, pp. 149-178.

[2] K. Nadaoka, M. Hino, Y. Koyano, "Structure of the turbulent flow field under breaking waves in the surf zone", Journal of Fluid Mechanics, 1989, Vol. 204, pp. 359-387.

[3] F. C. K. Ting, "Large-scale turbulence under a solitary wave", Coastal Engineering, 2006, Vol. 53, pp. 441-462

[4] Y. Watanabe, H. Saeki, R. J. Hosking, "Three-dimensional vortex structures under the breaking waves", Journal of Fluid Mechanics, 2005, Vol. 545, pp. 291-328.

[5] J. J. Monaghan, "Simulating free surface flows with SPH", Journal of Computational Physics", 110, 399-406, 1994.

[6] A. Hérault, G. Bilotta, R. A. Dalrymple, "SPH on GPU with CUDA", Journal of Hydraulic Research, 2010, Vol. 48, pp. 74-79.

[7] M. Brachet, M. Meneguzzi, H. Plitano, and P. Sulem, "The dynamics of freely decaying two-dimensional turbulence", Journal of Fluid Mechanics, 1988, Vol. 194, pp. 333-349.

[8] A. Babiano, C. Basdevant, B. Legras, and R. Sadourny, "Vorticity and passive-scalar dynamics in two-dimensional turbulence", Journal of Fluid Mechanics, 1987, Vol.183, pp. 379-397.

[9] J. McWilliams, "The vortices of two-dimensional turbulence", Journal of Fluid Mechanics, 1990, Vol. 219, pp. 361-385.

[10] S. I. Green, "Fluid vortices", Kluwer academic publishers, 1995.

[11] J. Jeong, F. Hussain, "On the identification of a vortex", Journal of fluid mechanics, 1995, Vol. 285, pp. 69-94.

[12] J. C. R. Hunt, A. Wray, P. Moin, "Eddies, stream and convergence zones in turbulent flows", Center for turbulence research report, 1988, CTR-S88.

[13] J. J. Monaghan and J.B. Kajtar, "SPH particle boundary forces for arbitrary boundaries", Computer Physics Communications, 2009, Vol. 180, , pp. 1811-1820.

[14] R.A. Dalrymple, B.D. Rogers, "Numerical modeling of water waves with the SPH method", Coastal Engineering, 2006, Vol. 53, pp. 141-147.